Seismic Moment, Seismic Energy, and Source Duration of Slow Earthquakes: Application of Brownian slow earthquake model to three major subduction zones

Satoshi Ide, Julie Maury

AGU100 ADVANCING EARTH AND SPACE SCIENCE

Geophysical Research Letters

RESEARCH LETTER
10.1002/2018GL077461

Key Points:
- The Brownian slow earthquake (BSE) model provides theoretical relationships among seismic moment, seismic energy, and source duration
- These theoretical relationships are compared with observations of slow earthquakes in the Japan, Mexico, and Cascadia subduction zones
- A BSE model with a non-Gaussian fluctuation can explain the observation of near-constant duration in isolated low-frequency earthquakes

Supporting Information:
- Supporting Information S1

Correspondence to:
S. Ide,
ide@eps.s.u-tokyo.ac.jp

Citation:
Ide, S., & Maury, J. (2018). Seismic moment, seismic energy, and source duration of slow earthquakes: Application of Brownian slow earthquake model to three major subduction zones. *Geophysical Research Letters*, *45*, 3059–3067. https://doi.org/10.1002/2018GL077461

Received 4 FEB 2018
Accepted 27 MAR 2018
Accepted article online 6 APR 2018
Published online 13 APR 2018

Seismic Moment, Seismic Energy, and Source Duration of Slow Earthquakes: Application of Brownian slow earthquake model to three major subduction zones

Satoshi Ide[1] and **Julie Maury**[2]

[1]Department of Earth and Planetary Science, The University of Tokyo, Tokyo, Japan, [2]BRGM, Orléans, France

Abstract Tectonic tremors, low-frequency earthquakes, very low-frequency earthquakes, and slow slip events are all regarded as components of broadband slow earthquakes, which can be modeled as a stochastic process using Brownian motion. Here we show that the Brownian slow earthquake model provides theoretical relationships among the seismic moment, seismic energy, and source duration of slow earthquakes and that this model explains various estimates of these quantities in three major subduction zones: Japan, Cascadia, and Mexico. While the estimates for these three regions are similar at the seismological frequencies, the seismic moment rates are significantly different in the geodetic observation. This difference is ascribed to the difference in the characteristic times of the Brownian slow earthquake model, which is controlled by the width of the source area. We also show that the model can include non-Gaussian fluctuations, which better explains recent findings of a near-constant source duration for low-frequency earthquake families.

Plain Language Summary Slow earthquake is a group of strange earthquake-like phenomena recently discovered in many subduction zones. It can be called by different names such as tectonic tremors, low-frequency earthquakes, very low-frequency earthquakes, and slow slip events, but actually considered as a very broadband phenomenon with various characteristic periods from ~0.1 s to ~1 year. This paper provides a theoretical model to explain various characteristics of slow earthquakes and compare the model with real observations in three major subduction zones: Japan, Cascadia, and Mexico. The interpretation of slow earthquake as a broadband phenomenon is essential for understanding the relation between earthquake rupture process and slow deformation in subduction zones.

1. Introduction

In various seismic regions worldwide, particularly in subduction zones, small and long-lasting seismic and geodetic signals have been detected and interpreted as radiating from underground shear deformation (e.g., Beroza & Ide, 2011; Obara & Kato, 2016; Schwartz & Rokosky, 2007). These signals are recognized as successive tectonic tremors, impulsive low-frequency earthquakes (LFEs) at ~2–8 Hz, very low frequency (VLF) events with a characteristic frequency of ~0.01–0.05 Hz, and slow slip events (SSEs). There seems to be common scaling relationships between small- and large-scale sources (Ide et al., 2007), suggesting that these signals radiate from a very broadband underground shear slip that is spatially and temporally inseparable. If all signals radiate during the same process, we may call these events "broadband slow earthquakes".

To simulate such broadband slip phenomena, Ide (2008, 2010a) proposed a stochastic model with the random fluctuation of source size represented using a Brownian motion. This Brownian slow earthquake (BSE) model can explain several characteristics of slow earthquakes: constant seismic moment rate, constant seismic energy rate, flat velocity spectrum in a wide frequency range, diffusive migration behavior, and statistics of the tremor amplitude. This model predicts that tremor signals are often accompanied by VLF components. The VLF signals hidden in a broadband seismogram can be detected by stacking the broadband records relative to the tremor timing, as demonstrated for Nankai, Japan (Ide & Tanaka, 2014; Ide & Yabe, 2014), Taiwan (Ide et al., 2015), Cascadia (Ide, 2016), and Mexico (Maury et al., 2016, 2018). The model also explains the ratios between the tremor energy and VLF seismic moment, which are between 10^{-10} and 10^{-9}, and shows little change among regions (e.g., Maury et al., 2018). This value, which is commonly called scaled energy (Kanamori & Heaton, 2000), is much smaller than the ratio for ordinary earthquakes of ~10^{-5}.

However, recent observations seem to contradict this assumption of the BSE model. A family of LFEs shares near-constant source time functions (Bostock et al., 2015; Thomas et al., 2016). High-resolution images of tremor sources indicate a spatially characteristic location radiating tremors (Peng & Rubin, 2017; Rubin & Armbruster, 2013). These findings are not consistent with the uniform Gaussian random fluctuation assumed in the BSE model. However, according to the central limit theorem, Brownian motion is a macroscopic image of any random process, as long as its fluctuation has a finite variance. This study shows that the BSE model is also considered as a limit of the fluctuating slip on the plate interface.

The purpose of this study is to update the BSE model with the current knowledge of slow earthquakes. First, we review the model, providing additional explanations of the model that have not been clearly demonstrated in previous papers. We then compare the model predictions with real observations. We focus on three subduction zones where slow earthquakes are observed and well-studied: Nankai, Japan, Cascadia, and Mexico, and confirm that the model is consistent with slow earthquake processes in these regions. This result demonstrates that the BSE model is useful for characterizing the observed differences among these regions.

2. Brownian Slow Earthquake Model

The slip region of SSEs has been determined using geodetic data (e.g., Bartlow et al., 2011; Radiguet et al., 2011; Yoshioka et al., 2015). The change is usually smooth, mainly due to the low resolution of the geodetic data. Tremors associated with these SSEs show a highly complex migration pattern, including fast transient migration (e.g., Houston et al., 2011; Shelly et al., 2007). Mechanically, both phenomena consist of shear slip on almost the same plane, and it would be reasonable to assume that the area hosting the shear slip is changing with time. The shape of the slip area is unknown, consisting of either one continuous region or numerous scattered small patches. Regardless, the size and location of the slip area change with time as a random fluctuation (Figure 1). It is possible to assign a characteristic size (linear dimension) of the total slip area as a random variable r, with an area $S = Cr^2$, where C is a constant characterizing the geometry, and $C = \pi$ represents the original model of Ide (2008).

The seismic moment rate is defined as the product of the rigidity μ, the area S, and the average slip rate v_{slip}. The variation in slip rate during slow earthquakes is poorly understood. The simplest assumption is a constant v_{slip}, which leads to a seismic moment rate $\dot{M}_o = C\mu v_{\mathrm{slip}} r^2 = C_s r^2$. While this is the S model assumed by Ide (2008), Ide (2010a) also considered a V model, where the slip rate increases with the size of the slip area, $v_{\mathrm{slip}} = \dot{\epsilon}_0 r$, and $\dot{\epsilon}_0$ is a constant strain rate. The seismic moment is then given as $\dot{M}_o = C\mu\dot{\epsilon}_0|r|^3 = C_v|r|^3$. These two models give slightly different scaling relations, but they can be treated similarly. Therefore, we primarily use the S model in the following sections.

The temporal change in r is expressed using a simple stochastic differential equation:

$$dr = -\alpha r dt + \sigma dB, \tag{1}$$

where α is the characteristic frequency (α^{-1} is the characteristic time) and σ is the magnitude of fluctuation. dB is a random variable with the standard Gaussian probability distribution, $N(0, dt)$. The square and cube of r are calculated as follows (e.g., Øksendal, 1998):

$$d\left(r^2\right) = \left(\sigma^2 - 2\alpha r^2\right)dt + 2\,\sigma r dB, \tag{2}$$

and

$$d\left(|r|^3\right) = \left(3\sigma^2|r| - 3\alpha|r|^3\right))dt + 3\sigma r^2 dB. \tag{3}$$

The long-term averages of $\dot{M}_o$ for the S and V models, respectively, are

$$E\left[\dot{M}_o\right] = C_s\frac{\sigma^2}{2\alpha}, \tag{4}$$

and

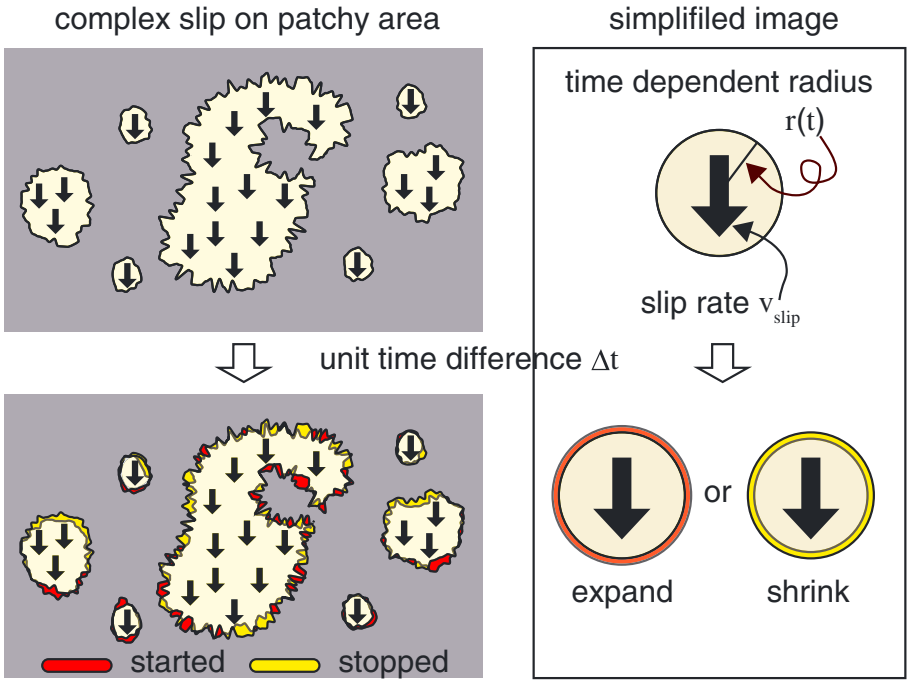

Figure 1. Schematic illustration of the Brownian slow earthquake model. The slip area changes at each time step, with slip starting and stopping at various points in the model. If we approximate the slip region with a circle, the change in slip area is indicated by the change in circle radius, which is represented as a stochastic differential equation.

$$E\left[\dot{M}_o\right] = C_v\sqrt{\frac{8}{\pi}}\left(\frac{\sigma^2}{2\alpha}\right)^{\frac{3}{2}}. \tag{5}$$

Thus, we obtain a constant moment rate, or the proportionality between the event duration and seismic moment, as shown by Ide et al. (2007). The constant moment rate depends on the characteristic time α^{-1} and the variance of fluctuation σ^2. Figures 2a and 2b show two examples of the moment rate function.

When the source size is small, the first term in equation (1) is negligible, and the process is a simple Brownian walk. For the S model, the expectation of r^2 is $\sigma^2 T$, where T is the duration of the event, measured between two successive moments of zero moment rate. Therefore, the seismic moment depends on the duration, taken as a power of 2 when T is much shorter than α^{-1} (Figure 2c). In the case of the V model, the expectation of r^3 is $2\sqrt{2}\sigma^3 T^{3/2}$. Therefore, the seismic moment depends on $T^{5/2}$. For a long time period and a large event, the moment rate in both models becomes independent of T. In the case of real phenomena, this change occurs by limiting the size of the slow earthquake zone (Ben-Zion, 2012; Gomberg, Agnew, & Schwartz, 2016; Ide, 2010a). The boundary between these two regimes is determined by the time required for growth to this size, where $T = \alpha^{-1}$ and $T = 0.63\alpha^{-1}$ for the S and V models, respectively. In principle, the duration of the event would be mathematically defined as the time between two successive moments when the moment rate is zero. However, real observations often consist of very small signals that are below the noise levels, such that the duration may be underestimated (Ide, 2008).

The seismic energy rate is proportional to the square of seismic moment acceleration,

$$\dot{E}_s = \frac{1}{10\pi\rho\beta^5}\int_{-\infty}^{\infty}\ddot{M}_o{}^2, \tag{6}$$

for a point source, neglecting P waves (e.g., Venkataraman & Kanamori, 2004), where ρ is the density and β is the S wave velocity. The expectations for the S and V models, respectively, are given as

$$E\left[\dot{E}_s\right] = C_s^2\frac{\sigma^4}{5\pi\rho\beta^5\alpha\Delta t}, \tag{7}$$

and

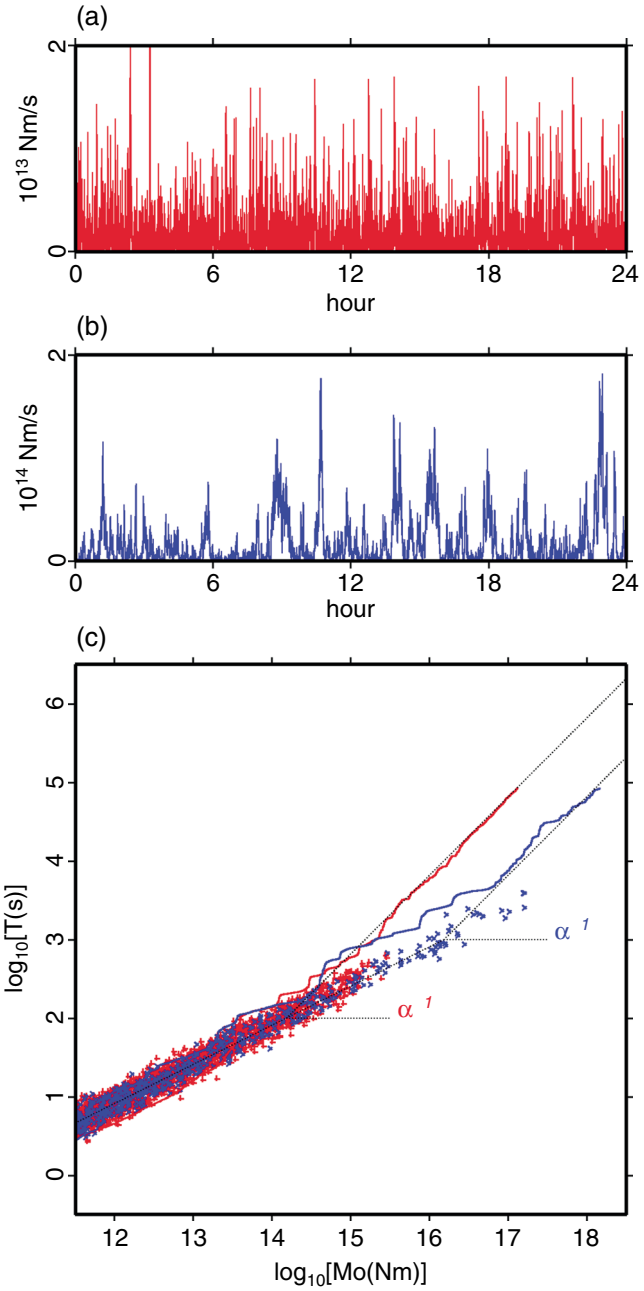

Figure 2. Moment rate function and moment rate spectra. (a) Moment rate function calculated for a Brownian slow earthquake model (S model). α^{-1} = 100 s, σ = 400 m/s$^{1/2}$, Δt = 0.05 s, and C_s = 1.9 × 10^5 N/ms. (b) As for (a), but with α^{-1} = 1, 000 s. (c) Relationship between seismic moment and duration. The red and blue lines show the cumulative moments for (a) and (b), respectively. The red and blue crosses are estimated for the events, determined between two successive moments of zero moment rate. The gray dotted lines are the predictions from the Brownian slow earthquake model.

$$E\left[\dot{E}_s\right] = C_v^2 \frac{27\sigma^6}{40\pi\rho\beta^5\alpha^2\Delta t}, \tag{8}$$

where Δt is introduced as the time step of the stochastic process, as the shortest time scale of the microscopic physical processes, which we cannot identify at this moment. The candidate would be inelastic process with a characteristic time, such as viscous friction, plastic deformation, and fluid or thermal diffusion in the source region. Because of this uncertainty, very precise discussion of energy is meaningless. The Δt practically determines the resolution limit, or the highest frequency represented in the model, which is related to the spectrum of the BSE model. The ratio between the energy rate and moment rate is constant, given as

$$\frac{E\left[\dot{E}_s\right]}{E\left[\dot{M}_o\right]} = C_s \frac{2\sigma^2}{5\pi\rho\beta^5\Delta t}, \tag{9}$$

for the S model.

3. Comparison With Observations

Figure 3a shows the seismic moment and duration estimated for SSEs and VLF events in three well-studied subduction zones: Japan, Cascadia, and Mexico. The seismic moment rate estimated for western Japan (Sekine et al., 2010) has a relatively small scatter, with the differences among the western Shikoku, Kii, and Tokai regions being 2.7 ± 1.1 × 10^{12}, 2.0 ± 0.6 × 10^{12}, and 1.2 ± 0.7 × 10^{12} Nm/s, respectively. These values are comparable with an estimate of 1.4 ± 0.4 × 10^{12} Nm/s for 20 Cascadia SSEs (Schmidt & Gao, 2010). However, the seismic moment rates estimated by Wech et al. (2009) for four Cascadia SSEs, including the events reported by Schmidt and Gao (2010), are 4.1–6.8 × 10^{12} Nm/s. Although the source of this large discrepancy is unclear, it is probably in the assumptions in each method, such as elastic structure, source geometry, and the definition of duration, and not in the original GPS data. In Mexico, the moment rate is higher, being 7.2–16.1 × 10^{12} Nm/s for three large Guerrero events (Graham et al., 2016) and 2.5–2.8 × 10^{13} Nm/s for many M_w~7 events (Rousset et al., 2017). The results suggest that the moment rates for these SSEs exhibit an increasing trend across the three subduction zones, from Japan (lowest) to Mexico (highest).

The seismic moment and duration have also been estimated for VLF signals that have been stacked relative to the tremor timing (e.g., Ide & Yabe, 2014; Takeo et al., 2010). The moment magnitudes for these signals are in the range 2.2–3.0, which increases with duration (10–30 s), but the slope is much smaller than one. The moment rates for Japan, Cascadia, and Mexico are 0.3–2.0 × 10^{12} (Ide & Yabe, 2014), 0.2–1.5 × 10^{12} (Ide, 2016), and 0.2–1.0 × 10^{12} Nm/s (Maury et al., 2016), respectively (Figure 3a). Thus, the difference for VLF events among the three regions is much smaller than that for the SSEs. To the right of these groups of stacked VLF signals, there are groups of very long duration events, such as those observed at Kii, Japan (Ide et al., 2008), with magnitudes and durations of up to M_w 4 and 300 s, respectively, which yield a slope of about 1/2 or 1/2.5, as predicted from the BSE model. The isolated VLF earthquakes have been estimated as much shorter-duration events, possessing a magnitude range that is similar to the long-duration events. In western Shikoku, Matsuzawa et al. (2010) identified four VLF events with M_w 3.5 – 3.8 and durations of 18–27 s. Although the source duration is not presented, the estimate by Ghosh et al. (2015) for the Cascadia VLF events is similar in size. In Guerrero, Maury et al. (2016) found 11

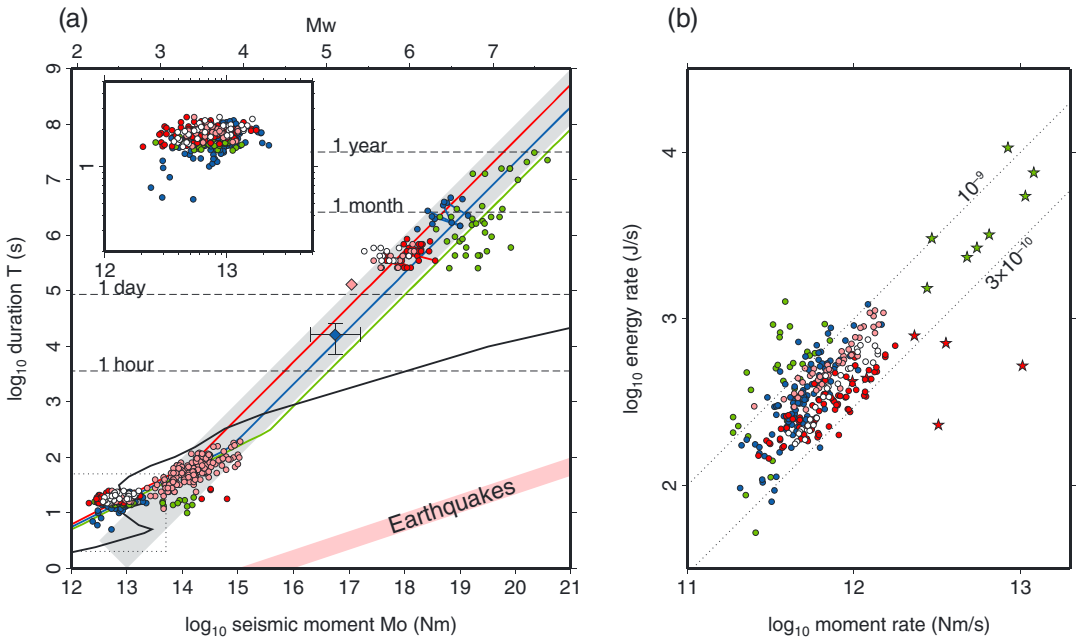

Figure 3. Comparison between the model and observations. The sources of all the data points are given in Table S1. (a) Comparison between the seismic moment and duration. The thick pink and gray lines are scaling relations for ordinary and slow earthquakes (Ide et al., 2007). The red, pink, white, blue, and green circles show estimates for the SSEs and VLFs in Shikoku, Kii, Tokai, Cascadia, and Mexico, respectively. Multiple estimates for one event are connected with a line. The pink and blue diamonds are the estimates of Itaba and Ando (2011) and Hawthorne et al. (2016), respectively. The red, blue, and green lines show the scaling relationship using the Brownian slow earthquake model, with α^{-1} = 75 (Japan), 150 (Cascadia), and 300 (Mexico), respectively. Inset is a close-up of the data points estimated for the stacked signals. The black curve shows the signature of typical noise, calculated using the new low noise model of Peterson (1993), which limits the detectability of the seismic signals. The horizontal location of this curve depends on the actual signal relative to the noise level of the observation. (b) Comparison between seismic moment and seismic energy. The color codes are the same as in (a), and the circles indicate estimates from the stacked signals and stars indicate estimates for the isolated events.

VLF events with M_w 3.0 – 3.4 and durations of 10–19 s. Thus, the moment rates for these events are 10^{13} Nm/s, approximately an order of magnitude higher than those from the stacked VLF signals. The main reason for this difference is probably that the independent VLF events (red and greed dots at M_w 3 – 4 in Figure 3a) correspond to rare large impulsive moment releases that are identified independently, whereas the stacking procedure averages various events.

Few observations have been made in the frequency range between these two groups of well-studied phenomena (VLF events and SSEs). Using highly sensitive strainmeters, Itaba and Ando (2011) found a M_w 5.3 SSE with a duration of 1.5 days and a moment rate of 0.9×10^{12} Nm/s in Kii, Japan. Hawthorne et al. (2016) estimated the seismic moment of SSEs during rapid tremor reversal of 2–8 hr for M_w 5.1 events, which equates to a moment rate of 2.8×10^{12} Nm/s for $T = 5$ hr. These values are similar to those estimated for larger SSEs. We can draw moment rate lines predicted by the BSE model with selected parameters to explain all the observations, extending from the VLF scale to the SSE scale (colored lines in Figure 3a). The lines are identical in the VLF scale but differ by factors of 2–5 in the SSE scale. This disparity reflects the differences in the characteristic time α^{-1}, which is assumed to be 75, 150, and 300 s for Japan, Cascadia, and Mexico, respectively, although these values are poorly constrained.

The seismic energy is another observable quantity but is less commonly analyzed and possesses large uncertainties due to the difficulties in calibrating the site amplification factors at observational sites. Note that the observable seismic energy is usually limited in the tremor band, which is a part of entire energy defined in (6), and the contribution from the frequencies outside of this band may change the value by some factor. Figure 3b compares the seismic moment rate and seismic energy rate values, modified from the compilation of Maury et al. (2018). These estimates are obtained from independent VLF events or the stacked VLF seismograms. The energy rate increases with the moment rate, and the ratios of the former to the latter, that is, the scaled energy, lie between 3×10^{-10} and 10^{-9}, yielding almost constant values, as expected from equation (9). Figure 3b also includes the data of Maeda and Obara (2009) for six SSEs with durations of

8–13 days, indicated by red stars. The scaled energy is slightly smaller for the SSEs, indicating a process that is not included in the BSE model. However, this difference may not be significant, given the large difference in the time scales of the phenomena, which is more than four orders of magnitude.

It should be noted that the energy rate divided by the square of the moment rate depends only the time constant (α^{-1} for long events), where

$$\frac{E\left[\dot{E}_s\right]}{E\left[\dot{M}_o\right]^2} = \frac{4\alpha}{5\pi\rho\beta^5\Delta t}, \tag{10}$$

For a short event, α^{-1} should be substituted by T. Here we assume that ρ = 2,700 kg/m^3 and β = 3,500 m/s. Since the maximum frequency of tremor is 3–8 Hz in Cascadia (Zhang et al., 2011), we may also assume $\Delta t = (\pi f_H)^{-1}$ = 0.05 s. This ratio is estimated to be ~10^{-20}–10^{-22} for the stacked VLF signals, yielding α^{-1} = 0.3 – 30 s, which is comparable to or shorter than the source durations determined for these stacked waveforms. However, the estimates reported by Maeda and Obara (2009) suggest that α^{-1} varies between 10 and 750 s, and our assumed α^{-1} values for the three subduction zones fall within this range.

We then estimate the other parameters in the BSE model. As mentioned above, among the three subduction zones, α^{-1} increases from Japan to Cascadia to Mexico. The maximum width of the tremor zone also increases in this order, as Maury et al. (2018) estimated widths of 23, 55, and 87 km, respectively. Given that the source radius is taken to be half of this maximum size, σ is estimated as 2,000–4,000 m/s$^{1/2}$. If the radius of the average slip area is just 10% of the maximum width, σ is then 400–800 m/s$^{1/2}$. Assuming a circular source, the moment rates in Japan, Cascadia, and Mexico are approximately 2.5, 5, and 10 × 10^{12} Nm/s, respectively, which allows us to then estimate v_{slip}. For the above two cases of large and small slip areas, v_{slip} is about 0.1 and 2 μm/s, respectively, for each of the three subduction zones. These rates are slow, but much faster than 1 nm/s, which is the relative plate velocity for each of these subduction zones.

4. Non-Gaussian Fluctuation in the BSE Model

We have assumed that the fluctuation term in the BSE models has a Gaussian distribution up to this point, but this is not an essential assumption of the model. This fluctuation can be regarded as either the start or end of the isolated LFEs, or the acceleration or deceleration of slip radiating from continuous tremor. Recent observations suggested that characteristic tiny slip events frequently occur in slow earthquake regions. One example is the observation of LFEs with almost constant duration (Bostock et al., 2015; Thomas et al., 2016). The stability of the tremor source locations in different episodes (Rubin & Armbruster, 2013) provides further evidence of this characteristic structure. The diversity of spatial characteristics in tremor regions was also suggested by the estimation of tremor duration, tidal sensitivity, and seismic energy radiation (Ide, 2010b; Yabe & Ide, 2014). There is no convincing reason to assume a uniform Gaussian distribution for the entirety of these phenomena. Rather, some spatially characteristic distribution of the fluctuation would be more appropriate.

The fluctuation dB in equation (1) can thus be substituted by other distributions. Since an LFE radiates moderate seismic energy, we may consider a power law type distribution, which is commonly employed in earthquakes statistics. Here we choose a double Gamma distribution, for which the probability density function is

$$\mathrm{pdf}(x) = \frac{1}{2b^a\Gamma(a)}|x|^{a-1}e^{-\frac{|x|}{b}}, \tag{11}$$

with a standard deviation of $b\sqrt{a(a+1)}$. Figure 4 compares the BSE models using this distribution with the original model. The moment rate functions were computed using this distribution, with the simulated observations in the high frequency (tremor) and VLF ranges. While the double Gamma distribution has much longer tails than the Gaussian distribution, it is difficult to distinguish between the two models in terms of the moment rate functions for 1 hr and the observed seismic waves in the VLF range. This outcome is

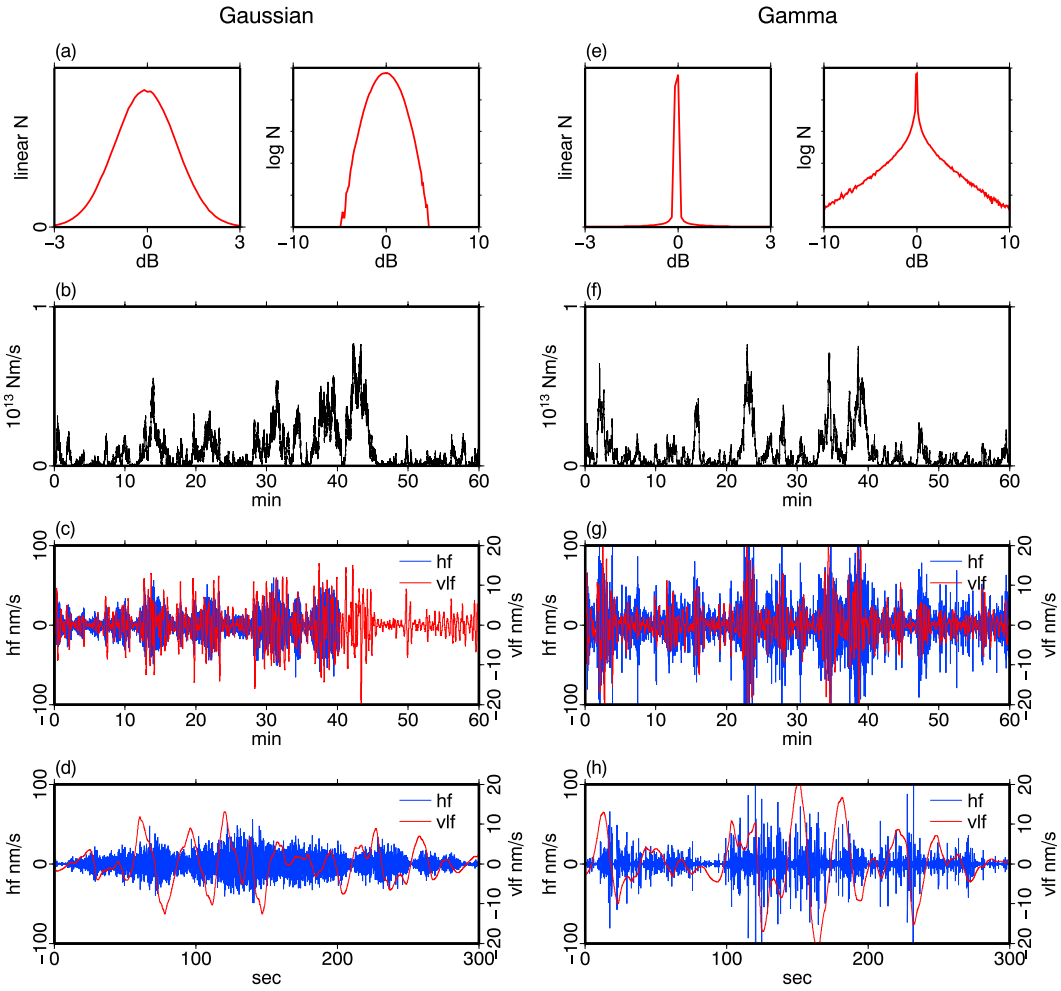

Figure 4. Comparison of the original Brownian slow earthquake model (S model) and a model using a double Gamma distribution as the fluctuation term. (a) Probability density distribution of the standard normal distribution shown in linear and semilog plots. (b) Moment rate function for 1 hr. (c) Simulated velocity waves filtered in the high-frequency band (blue) and VLF band (red). (d) Close-up of the first 300 s in (c). (e–h) As for (a–d), but for the double Gamma distribution, with $a = 0.1$ and $b = 3.02$. The simulated waves are calculated assuming a point source located 40 km from the observing point in a homogeneous medium, with $\rho = 2{,}700$ kg/m^3 and $\beta = 3{,}500$ m/s. In both models, $\alpha^{-1} = 100$ s, $\sigma = 400$ m/s$^{1/2}$, $\Delta t = 0.05$ s, and $C_s = 1.9 \times 10^5$ N/ms.

expected from the central limit theorem, and any distribution should yield similar results as long as the variance is defined.

At a finer scale, we see a discrepancy identified as several spikey pulses in the high-frequency records (Figures 4h and S1). These pulses would be recognized as isolated LFEs if they were observed in nature. The temporal correlation between these spikey pulses and VLF signals is not always clear. Each spike is produced by a rare impulsive fluctuation characterized by the long tail of a power law type distribution, and the amplitude soon decreases without a subsequent increase. Therefore, the source time function of these "events" is comparable to twice the time step, where $2\Delta t = 0.1$ s in Figure S1, with a slight dependence on amplitude. This result is similar to that reported by Bostock et al. (2015). The visibility of such isolated LFEs depends on the nature of the fluctuation term.

The temporal consistency during a sequence is also important. While the BSE model assumes constant fluctuations, the moment release of natural events is generally more intermittent. Based on the observation of SSEs in Cascadia and Mexico, Frank (2016) suggested that the SSE process involves repeated seismic and interseismic periods over an apparently continuous sequence. As shown in the examples in Figure 2b, the BSE models can mimic some of this switching process as a random fluctuation with a large time constant α^{-1}. More explicit interseismic periods might be necessary, although it is difficult to discuss due to noise.

5. Conclusion

This paper provides an update to the BSE model, a stochastic process that governs the whole spectrum of slow earthquakes, and a comparison with natural phenomena observed in the subduction zones of Japan, Cascadia, and Mexico. A few parameters in the BSE model can explain various observations in each region. The relationship between seismic moment and event duration is well explained by BSE models with different time constants, which also correlate well with the width of each source region.

The model is applicable with any random fluctuations, as long as they show a finite variance. The real source region must have a heterogeneous structure. Nevertheless, for frequencies lower than the VLF range, the heterogeneity is smoothed out and we observe the relatively averaged nature of the source, which is well represented by BSE models with a Gaussian fluctuation. In this sense, the model can include many LFEs as unit structures of fluctuation that represent VLF signals and much longer-period phenomena. A similar idea was presented by Gomberg, Wech, et al. (2016), which we can regard as a special case of the BSE model. Since real phenomena occur in 2-D or 3-D space, a simple 1-D time domain model may not be applicable, and a more realistic simulation of diffusional phenomena will be required for a more complete understanding of these processes.

Acknowledgments
This research was supported by JSPS Kakenhi (16H02219), MEXT Kakenhi (16H06477), and the Earthquake and Volcano Hazards Observation and Research Program of MEXT. The data used in Figure 3 are listed in Tables S1 and S2.

References

Bartlow, N. M., Miyazaki, S., Bradley, A. M., & Segall, P. (2011). Space-time correlation of slip and tremor during the 2009 Cascadia slow slip event. *Geophysical Research Letters*, *38*(18), L18309. https://doi.org/10.1029/2011GL048714

Ben-Zion, Y. (2012). Episodic tremor and slip on a frictional interface with critical zero weakening in elastic solid. *Geophysical Journal International*, *189*(2), 1159–1168. https://doi.org/10.1111/j.1365-246X.2012.05422.x

Beroza, G. C., & Ide, S. (2011). Slow earthquakes and nonvolcanic tremor. *Annual Review of Earth and Planetary Sciences*, *39*(1), 271–296. https://doi.org/10.1146/annurev-earth-040809-152531

Bostock, M. G., Thomas, A. M., Savard, G., Chuang, L., & Rubin, A. M. (2015). Magnitudes and moment-duration scaling of low-frequency earthquakes beneath southern Vancouver Island. *Journal of Geophysical Research: Solid Earth*, *120*, 6329–6350. https://doi.org/10.1002/2015JB012195

Frank, W. B. (2016). Slow slip hidden in the noise: The intermittence of tectonic release. *Geophysical Research Letters*, *43*(19), 10,125–10,133. https://doi.org/10.1002/2016GL069537

Ghosh, A., Huesca-Pérez, E., Brodsky, E., & Ito, Y. (2015). Very low frequency earthquakes in Cascadia migrate with tremor. *Geophysical Research Letters*, *42*(9), 3228–3232. https://doi.org/10.1002/2015GL063286

Gomberg, J., Agnew, D. C., & Schwartz, S. Y. (2016). Alternative source models of very low frequency events. *Journal of Geophysical Research: Solid Earth*, *121*(9), 6722–6740. https://doi.org/10.1002/2016JB013001

Gomberg, J., Wech, A., Creager, K., Obara, K., & Agnew, D. (2016). Reconsidering earthquake scaling. *Geophysical Research Letters*, *43*(12), 6243–6251. https://doi.org/10.1002/2016GL069967

Graham, S., DeMets, C., Cabral-Cano, E., Kostoglodov, V., Rousset, B., Walpersdorf, A., et al. (2016). Slow slip history for the Mexico subduction zone: 2005 through 2011. *Pure and Applied Geophysics*, *173*(10–11), 3445–3465. https://doi.org/10.1007/s00024-015-1211-x

Hawthorne, J. C., Bostock, M. G., Royer, A. A., & Thomas, A. M. (2016). Variations in slow slip moment rate associated with rapid tremor reversals in Cascadia. *Geochemistry, Geophysics, Geosystems*, *17*(12), 4899–4919. https://doi.org/10.1002/2016GC006489

Houston, H., Delbridge, B. G., Wech, A. G., & Creager, K. C. (2011). Rapid tremor reversals in Cascadia generated by a weakened plate interface. *Nature Geoscience*, *4*(6), 404. https://doi.org/10.1038/ngeo1157

Ide, S. (2008). A Brownian walk model for slow earthquakes. *Geophysical Research Letters*, *35*(17), 3–7. L17301. https://doi.org/10.1029/2008GL034821

Ide, S. (2010a). Quantifying the time function of nonvolcanic tremor based on a stochastic model. *Journal of Geophysical Research*, *115*, B08313. https://doi.org/10.1029/2009JB000829

Ide, S. (2010b). Striations, duration, migration and tidal response in deep tremor. *Nature*, *466*(7304), 356–359. https://doi.org/10.1038/nature09251

Ide, S. (2016). Characteristics of slow earthquakes in the very low frequency band: Application to the Cascadia subduction zone. *Journal of Geophysical Research: Solid Earth*, *121*, 5942–5952. https://doi.org/10.1002/2016JB013085

Ide, S., Beroza, G. C., Shelly, D. R., & Uchide, T. (2007). A scaling law for slow earthquakes. *Nature*, *447*(7140), 76–79. https://doi.org/10.1038/nature05780

Ide, S., Imanishi, K., Yoshida, Y., Beroza, G. C., & Shelly, D. R. (2008). Bridging the gap between seismically and geodetically detected slow earthquakes. *Geophysical Research Letters*, *35*, L10305. https://doi.org/10.1029/2008GL034014

Ide, S., & Tanaka, Y. (2014). Controls on plate motion by oscillating tidal stress: Evidence from deep tremors in western Japan. *Geophysical Research Letters*, *41*(11), 3842–3850. https://doi.org/10.1002/2014GL060035

Ide, S., & Yabe, S. (2014). Universality of slow earthquakes in the very low frequency band. *Geophysical Research Letters*, *41*(8), 2786–2793. https://doi.org/10.1002/2014GL059712

Ide, S., Yabe, S., Tai, H.-J., & Chen, K. H. (2015). Thrust-type focal mechanisms of tectonic tremors in Taiwan: Evidence of subduction. *Geophysical Research Letters*, *42*(9), 3248–3256. https://doi.org/10.1002/2015GL063794

Itaba, S., & Ando, R. (2011). A slow slip event triggered by teleseismic surface waves. *Geophysical Research Letters*, *38*, L21306. https://doi.org/10.1029/2011GL049593

Kanamori, H., & Heaton, T. H. (2000). Microscopic and macroscopic physics of earthquakes. In J. Rundle, D. Turcotte, & W. Klein (Eds.), *Geocomplexity and the Physics of Earthquakes, Geophysical Monograph Series* (Vol. 120, pp. 147–163). Washington, DC: American Geophysical Union. https://doi.org/10.1029/GM120p0147

Maeda, T., & Obara, K. (2009). Spatiotemporal distribution of seismic energy radiation from low-frequency tremor in western Shikoku, Japan. *Journal of Geophysical Research*, *114*, B00A09. https://doi.org/10.1029/2008JB006043

Matsuzawa, T., Hirose, H., Shibazaki, B., & Obara, K. (2010). Modeling short- and long-term slow slip events in the seismic cycles of large subduction earthquakes. *Journal of Geophysical Research*, *115*, B12301. https://doi.org/10.1029/2010JB007566

Maury, J., Ide, S., Cruz-Atienza, V. M., & Kostoglodov, V. (2018). Spatiotemporal variations in slow earthquakes along the Mexican subduction zone. *Journal of Geophysical Research: Solid Earth*, *123*, 1559–1575. https://doi.org/10.1002/2017JB014690

Maury, J., Ide, S., Cruz-Atienza, V. M., Kostoglodov, V., Gonzáles-Molina, G., & Péres-Campos, X. (2016). Comparative study of tectonic tremor locations: Characterization of slow earthquakes in Guerrero, Mexico. *Journal of Geophysical Research: Solid Earth*, *121*, 5136–5151. https://doi.org/10.1002/2016JB013027

Obara, K., & Kato, A. (2016). Connecting slow earthquakes to huge earthquakes. *Science*, *353*(6296), 253–257. https://doi.org/10.1126/science.aaf1512

Øksendal, B. K. (1998). *Stochastic differential equations* (5th ed.). Berlin, Germany: Springer. https://doi.org/10.1007/978-3-662-03620-4

Peng, Y., & Rubin, A. M. (2017). Intermittent tremor migrations beneath Guerrero, Mexico, and implications for fault healing within the slow slip zone. *Geophysical Research Letters*, *44*(2), 760–770. https://doi.org/10.1002/2016GL071614

Peterson, J. (1993). Observations and modeling of seismic background noise. U.S. Geological Survey Open File Report, 93–322.

Radiguet, M., Cotton, F., Vergnolle, M., Campillo, M., Valette, B., Kostoglodov, V., & Cotte, N. (2011). Spatial and temporal evolution of a long term slow slip event: The 2006 Guerrero slow slip event. *Geophysical Journal International*, *184*(2), 816–828. https://doi.org/10.1111/j.1365-246X.2010.04866.x

Rousset, B., Campillo, M., Lasserre, C., Frank, W. B., Cotte, N., Walpersdorf, A., et al. (2017). A geodetic matched-filter search for slow slip with application to the Mexico subduction zone. *Journal of Geophysical Research: Solid Earth*, *122*, 10,498–10,514. https://doi.org/10.1002/2017JB014448

Rubin, A. M., & Armbruster, J. G. (2013). Imaging slow slip fronts in Cascadia with high precision cross-station tremor locations. *Geochemistry, Geophysics, Geosystems*, *14*(12), 5371–5392. https://doi.org/10.1002/2013GC005031

Schmidt, D. A., & Gao, H. (2010). Source parameters and time-dependent slip distributions of slow slip events on the Cascadia subduction zone from 1998 to 2008. *Journal of Geophysical Research*, *115*, B00A18. https://doi.org/10.1029/2008JB006045

Schwartz, S. Y., & Rokosky, J. M. (2007). Slow slip events and seismic tremor at circum-Pacific subduction zones. *Reviews of Geophysics*, *45*(3), RG3004. https://doi.org/10.1029/2006RG000208

Sekine, S., Hirose, H., & Obara, K. (2010). Along-strike variations in short-term slow slip events in the southwest Japan subduction zone. *Journal of Geophysical Research*, *115*, B00A27. https://doi.org/10.1029/2008JB006059

Shelly, D. R., Beroza, G. C., & Ide, S. (2007). Non-volcanic tremor and low-frequency earthquake swarms. *Nature*, *446*(7133), 305–307. https://doi.org/10.1038/nature05666

Takeo, A., Idehara, K., Iritani, R., Tonegawa, T., Nagaoka, Y., Nishida, K., et al. (2010). Very broadband analysis of a swarm of very low frequency earthquakes and tremors beneath Kii Peninsula, SW Japan. *Geophysical Research Letters*, *37*, L06311. https://doi.org/10.1029/2010GL042586

Thomas, A. M., Beroza, G. C., & Shelly, D. R. (2016). Constraints on the source parameters of low-frequency earthquakes on the San Andreas Fault. *Geophysical Research Letters*, *43*(4), 1464–1471. https://doi.org/10.1002/2015GL067173

Venkataraman, A., & Kanamori, H. (2004). Effect of directivity on estimates of radiated seismic energy. *Journal of Geophysical Research*, *109*, B04301. https://doi.org/10.1029/2003JB002548

Wech, A. G., Creager, K. C., & Melbourne, T. I. (2009). Seismic and geodetic constraints on Cascadia slow slip. *Journal of Geophysical Research*, *114*, B10316. https://doi.org/10.1029/2008JB006090

Yabe, S., & Ide, S. (2014). Spatial distribution of seismic energy rate of tectonic tremors in subduction zones. *Journal of Geophysical Research: Solid Earth*, *119*, 8171–8185. https://doi.org/10.1002/2014JB011383

Yoshioka, S., Matsuoka, Y., & Ide, S. (2015). Spatiotemporal slip distributions of three long-term slow slip events beneath the Bungo Channel, southwest Japan, inferred from inversion analyses of GPS data. *Geophysical Journal International*, *201*(3), 1437–1455. https://doi.org/10.1093/gji/ggv022

Zhang, J., Gerstoft, P., Shearer, P. M., Yao, H., Vidale, J. E., Houston, H., & Ghosh, A. (2011). Cascadia tremor spectra: Low corner frequencies and earthquake-like high-frequency falloff. *Geochemistry, Geophysics, Geosystems*, *12*(10), Q10007. https://doi.org/10.1029/2011GC003759